Published in final edited form as:
Arch Toxicol. 2011 July ; 85(7): 787–798. doi:10.1007/s00204-010-0627-4.

Differential Stability of Lead Sulfide Nanoparticles Influences Biological Responses in Embryonic Zebrafish

Lisa Truong[1,2], **Ian S Moody**[3], **Dylan P Stankus**[2,4], **Jeffrey A Nason**[2,4], **Mark C Lonergan**[2,3], and **Robert L Tanguay**[1,2,*]

[1]Department of Environmental and Molecular Toxicology, Oregon State University, Corvallis, OR 97331

[2]Safer Nanomaterials and Nanomanufacturing Initiative, Oregon Nanoscience and Microtechnologies Institute, Corvallis

[3]Department of Chemistry and the Materials Science Institute, University of Oregon, Eugene, Oregon 97403

[4]School of Chemical, Biological and Environmental Engineering, Oregon State University, Corvallis, OR 97331

Abstract

As the number of nanoparticle-based products increase in the marketplace, there will be increased potential for human exposures to these engineered materials throughout the product life cycle. We currently lack sufficient data to understand or predict the inherent nanomaterial characteristics that drive nanomaterial-biological interactions and responses. In this study, we utilized the embryonic zebrafish *(Danio rerio)* model to investigate the importance of nanoparticle (NP) surface functionalization, in particular as it pertains to nanoparticle stability, on *in vivo* biological responses. This is a comparative study where two lead sulfide nanoparticles (PbS-NPs) with nearly identical core sizes, but functionalized with either sodium 3-mercaptopropanesulfonate (MT), or sodium 2,3-dimercaptopropanesulfonate (DT) ligand were used. Developmental exposures and assessments revealed differential biological responses to these engineered nanoparticles. Exposures beginning at 6 hours post fertilization (hpf) to MT-functionalized nanoparticles (PbS-MT) led to 100% mortality by 120 hpf while exposure to DT-functionalized nanoparticles (PbS-DT) produced less than a 5% incident in mortality at the same concentration. Exposure to the MT and DT ligands themselves did not produce adverse developmental effects when not coupled to the NP core. Following exposure, we confirmed that the embryos took up both PbS-MT and PbS-DT material using Inductively Coupled Plasma – Mass Spectrometry (ICP-MS). The stability of the nanoparticles in the aqueous solution was also characterized. The nanoparticles decompose and precipitate upon exposure to air. Soluble lead ions were observed following nanoparticle precipitation and in greater concentration for the PbS-MT sample compared to the PbS-DT sample. These studies demonstrate that *in vivo* assessments can be effectively used to characterize the role of NP surface functionalization in predicting biological responses.

Keywords

lead sulfide; nanoparticle; nanomaterial-biological interaction; toxicity; stability

*Correspondence to: Robert Tanguay, Ph.D. Nanotoxicology Laboratory, Department of Environmental and Molecular Toxicology, ALS 1007, Oregon State University, Corvallis, OR 97331. Robert.Tanguay@oregonstate.edu, Telephone: 1-541-737-6514, Fax: 1-541-737-7966.

Introduction

Nanoparticles (NPs) are becoming ubiquitous as they are incorporated into an increasing number of commercial products. Exploiting their unique material properties, nanoparticle-based applications will undoubtedly revolutionize many features of our lives. Nanotechnology is used in a broad spectrum of applications, encompassing cosmetics, biomedical supplies, fluorescent bioimaging, and electronics (Minchin and Martin 2010; Usenko et al. 2007; Bharali et al. 2009; Newman et al. 2009).

Despite the rapid growth of the nanotechnology industry, research into interactions of nanoparticles with environmental and biological systems has not kept pace with material development. Currently, the interplay between nanoscale materials and biological systems is poorly understood, and hazards have not been fully evaluated. Without toxicological data regarding the biocompatibility of nanoparticles, it is impossible to identify risk associated with nanoparticle exposure. An efficient testing method, if proven predictive, would help fill these critical data gaps.

Various biological models have been proposed for toxicological assessments including *in vitro* and *in vivo* methodologies. *In vitro* studies, such as cell culture, are rapid, efficient, and low-cost. However, results from these studies are often difficult to translate to the whole organism. Utilizing *in vivo* models may offer a more immediately relevant platform for translational studies (Teraoka et al. 2003; den Hertog 2005; Hall et al. 2007). The widely accepted rodent model is both cost and labor intensive; it requires extensive animal care facilities and significant quantities of test materials for the toxicity assessments. A powerful alternative is the zebrafish model (Parng 2005), which is now widely accepted for mechanistic-based toxicological studies (Haendel et al. 2004; Hill et al. 2005; Ton et al. 2006; Usenko et al. 2007; Furgeson et al. 2009).

Zebrafish have a high degree of homology to the human genome and share many cellular, anatomical, and physiological characteristics with other vertebrates (Barbazuk et al. 2000). Their small size, rapid development, and short life cycle make zebrafish an ideal rapid assessment model, which is needed to provide solid and crucial toxicological data (Dodd et al. 2000; Rubinstein 2003; and Yang et al. 2003). Female zebrafish are capable of producing hundreds of embryos a day, thereby providing statistical power to the analysis. Embryos develop externally and are transparent for the first few days of their development, allowing for non-invasive assessments (Kimmel et al. 1995). The small quantity needed to fully evaluate biological responses to a novel engineered nanoparticle (typically, less than 1 mg) is also a major advantage for “green by design” synthesis strategies. With other models, material requirements are orders of magnitude greater. This combination of rapid assessments, unlimited embryos, and minimal material needs, makes the zebrafish model ideal for investigation of nanomaterial-biological interactions.

Lead sulfide nanoparticles (PbS-NPs) have been increasingly developed and studied due to their unique electrical and optical properties. Like other semiconductor nanoparticles, they exhibit quantum confinement below a certain size threshold– the so-called, *quantum size effect* – that allows their optical and electrical properties to be precisely tuned with size. Lead sulfide, in particular, has shown promise as a material that is optically active in the near infrared (NIR) region of the electromagnetic spectrum. Sensitivity to this spectral window is critical for a variety of photonic applications, including single- and multi-junction solar cells (Koleilat et al. 2008 and McDonald et al. 2005), NIR photodetectors for telecommunications (Konstantatos et al. 2006), and NIR light-emitting diodes (LEDs) (Konstantatos et al. 2005). Additionally, solubilized PbS-NPs have been studied as fluorescent biomarkers that can take advantage of the transparent tissue window at

700-1000nm for *in vivo* cellular imaging (Hyun et al. 2007, Hinds et al. 2007, and Lim et al. 2003).

Despite increased interest in PbS-NPs as industrial materials, very little is known about their biological or environmental interactions. Compounds containing lead can induce a wide variety of adverse human effects (ATSDR 2007), such as genotoxicity (Zelikoff 1988), oxidative stress (Sharma 2010), and neurological effects (De Gennardo 1978). It is known that lead can affect multiple systems in the body, most notably the nervous system. Cardiovascular, immune, and reproductive systems as well as bones, teeth, and kidneys are also sensitive targets (White et al 2007). Lead sulfide (PbS) – *galena* – is an extensively mined ore, which is negligibly soluble in aqueous systems, making bioavailability in solutions limited. PbS can undergo decomposition processes, and reduced particle size is known to increase decomposition rates (Liu et al. 2009), which influences the amount of ionic lead available. To complicate the understanding of nanoparticle-biological interaction, nearly all colloidal nanoparticle preparation has organic stabilizing molecules, ligands, that bind to the surface of the core, passivate surface states, retard particle growth and agglomeration, and imbue the nanoparticles with solubility.

Toxicological studies on other nanoparticle systems have identified key structural features important to understanding nanomaterial-biological interactions (Kirchner et al. 2005; Kotov et al. 2009). One such feature, chemical composition of the nanoparticle core, has been identified as a good predictor of toxicity. Nanoparticles composed of known toxic metals for example cadmium (Samia et al. 2003; Kirchner et al. 2005) and silver (Wise et al. 2009)) – are generally more toxic than those composed of inert materials such as gold (Furgeson et al. 2009). Core size is also an important feature, with smaller particles of the same core material, generally more toxic than larger ones (Meng et al. 2007; Guo et al. 2008). Smaller particles are thought to interact more strongly with biological systems, either through enhanced cellular uptake, or through faster decomposition due to greater surface area-to-volume ratios compared to larger particles. In addition to the composition of the nanoparticle core, ligand shells can affect nanoparticle toxicity (Hoshino et al. 2004).

This wide array of variables can make correlation of structure-activity relationships difficult. The aim of this study was to isolate one of these variables – ligand head group as a key factor in nanoparticle stability, while keeping all other factors (core material, core size, and ligand tail group) constant. At the same time, we hoped to open investigation into the little understood toxicity of the technologically-relevant nanomaterial – PbS. Specifically, in this study, two types of water soluble PbS-NPs were tested in the embryonic zebrafish system. Both PbS-NP had similar core size (~3nm), and were functionalized with either a sodium 3-mercaptopropanesulfonate (MT) ligand, or its bidentate analogue – sodium 2,3-dimercaptopropanesulfonate (DT). These two ligands are structurally analogous; both ligands have the same carbon backbone and sulfonate tail group, and differ only in the head group – mono- vs. di- thiol, respectively. Prior studies on these nanoparticles revealed that the two ligands offered differential protection against oxidative decomposition, with MT-functionalized particles being less stable to precipitation (Moody et al. 2008). This feature made MT- and DT-capped nanoparticles a compelling set in which to study the effects of particle stability on nanoparticle toxicity, while keeping other structural features unchanged. Utilizing the zebrafish model to screen for developmental toxicity revealed that the different surface functionalizations of the nanoparticles produced different biological responses.

Materials and Methods

Nanoparticles

Materials—Lead (II) oxide (PbO); oleic acid (OLA, 90% technical grade); 1-octadecene (ODE, 90% technical grade); bis-(trimethylsilyl)sulfide; 3-mercaptopropanesulfonic acid, sodium salt (MT, 90%); and, 2,3-dimercaptopropanesulfonic acid, sodium salt, monohydrate (DT, 95%) were all purchased from Aldrich. Deuterium oxide was obtained from Cambridge Isotope Laboratories, Inc. Acetonitrile and toluene were distilled under nitrogen from P_2O_5 and Na/benzophenone, respectively, before use. Nanopure water and other solvents were deoxygenated either by sparging with nitrogen or freeze-pump-thaw degassing.

Synthesis of Lead Sulfide Nanoparticles (PbS-NPs)—Moody et al (2008) have previously reported this procedure. Briefly, PbO was dissolved in OLA and heated under vacuum to remove water and form lead oleate. To form PbS-NPs, a solution of bis-(trimethylsilyl) sulfide in ODE was quickly injected into the stirring mixture of lead oleate at 130°C under nitrogen. After cooling, the crude nanoparticle solution was purified by a series of precipitation-centrifugation-resuspension steps, using distilled toluene and methanol as the solvent and non-solvent, respectively. Oleic-acid capped PbS-NPs were then exchanged with either MT or DT ligands in a biphasic solution of toluene and water. Biphasic mixtures were manually shaken for one hour and then centrifuged. The organic layer, along with any remaining organic-soluble NPs, were removed from the aqueous layer and discarded. Thiol-functionalized NPs in the aqueous layer were washed with toluene to remove any remaining free OLA. To purify the nanoparticles, another series of precipitation-centrifugation-resuspension steps was performed using nanopure water and acetonitrile, as the solvent and non-solvent, respectively. A typical exchange procedure used equal volumes of a 25 mg/mL solution of PbS-OLA in toluene and either a 180 mM solution of MT or 78 mM solution of DT in water.

At all steps in the synthesis and exchange, standard air-free techniques were employed. Samples and reagents were stored under nitrogen in Schlenk flasks or centrifuge tubes with septa caps, and transferred via gas-tight syringes.

Physical Characterization of Nanoparticles

- **Near-Infrared (NIR) Absorption Spectroscopy-** Absorption spectra were measured on a Perkin-Elmer Lambda 19 UV/VIS/NIR Spectrophotometer. To reduce solvent absorption in the spectral window of interest, deuterium oxide was used in place of water for this measurement. Nanoparticle solutions were diluted to a concentration regime (~1 mg/mL) where a linear dependence of absorbance on concentration was observed.
- **Transmission Electron Microscopy (TEM)** – Samples of PbS-MT and PbS-DT were prepared using amine-functionalized “Smart Grids” obtained from Dune Sciences, Inc. To prepare, a “Smart-Grid” was floated atop a drop of dilute nanoparticle solution. After 10 seconds, the grid was dipped in deionized water to remove excess sample, then blotted dry from beneath with a Kimwipe. Images were taken using an FEI Titan 80-300 S/TEM microscope operating at 300 keV at 56k magnification and a pixel resolution of 2.58 pixels/nm.

  Size analysis was performed using ImageJ software. Image contrast was enhanced to the minimum level necessary for automated particle counting, and all images were processed identically. To improve contrast, a Gaussian blur function and bandpass filter were applied. Segmenting was achieved using the

"MultiThresholder" plug-in, utilizing the "Intermodes" method. Prior to automated counting, size and circularity constraints were used to remove large agglomerates from the count. The results of the automated particle analysis were checked against the original image. Particle diameter was taken to be the average of the major and minor axes of the ellipse fit.

- **Lead Analysis by Inductively Coupled Plasma –Optical Emission Spectrometry (ICP-OES) –** Three aliquots (50 μL each) for both fresh PbS-MT and PbS-DT (nominally, 3 mg/mL) were analyzed. Aliquots were digested with 196 μL of ultra pure nitric acid (HNO_3) (VWR: 87003-226) for 12 hours prior to analysis. The remaining nanoparticle solutions were then left to precipitate (age) under ambient conditions for five days. When precipitated, the nanoparticles from both solutions collected as insoluble agglomerates, leaving fractions of solubilized lead in the clear supernatant. For each aged sample, the supernatant was drawn off and centrifuged at 13,000 rpm for 10 minutes to remove any remaining nanoparticles. The centrifuged supernatant (50 μL) was then digested in the same manner as for the fresh nanoparticle solution aliquots (three replicates). Prior to sampling, each sample was diluted to 10 mL with Milli-Q water. Samples were vortexed and placed into autosampler racks prior to being analyzed. The ICP-OES was calibrated using a lead standard in 0.5% HNO_3 at seven concentrations (0.25, 0.5, 5, 10, 20, 35 and 50 ppm). The calibration curve created by the standard solutions had an R^2 value of 0.996. Measured concentrations of lead in the undiluted nanoparticle solutions were back-calculated from the lead content determined by ICP-OES in the aliquots, and the dilution factor. The percentage of recovered lead was calculated from the ratio of the measured concentration to the theoretical concentration. The theoretical concentration is based on several assumptions: the nanoparticles are spherical, the Pb to S ratio in the core is 1:1, and the surface Pb atom to ligand ratio is 1:1. Given these assumptions, the calculated theoretical concentrations of lead in the fresh solutions were 2189 ppm for PbS-MT and 2129 ppm for PbS-DT.
- **Dynamic Light Scattering (DLS)** – Equal concentrations (40 ppm) of PbS-MT and PbS-DT were prepared by diluting aqueous nanoparticle stock solutions (20 mg/mL in deionized water) with fish water (FW). Immediately after dilution, solutions underwent a single pass through a 0.2μm filter to remove dust that could influence the scattering experiments. Hydrodynamic radii were taken as the average of three samples, and measured using a Brookhaven 90 Plus Particle Size Analyzer.

Zebrafish

Exposure Protocol—Embryonic zebrafish were obtained from a Tropical 5D strain of zebrafish (*Danio rerio*) reared in the Sinnhuber Aquatic Research Laboratory (SARL) at Oregon State University. Adults were kept at standard laboratory conditions of 28°C on a 14h light/10h dark photoperiod in fish water(FW) consisting of reverse osmosis water supplemented with a commercially available salt (Instant OceanR) to create a salinity of 600 microsiemen and sodium bicarbonate was added as needed to adjust the pH to 7.4. Zebrafish were group spawned and embryos were collected and staged as described by Kimmel et al (1995). To increase bioavailability, the chorion, an acellular envelope surrounding the embryo, was removed enzymatically with pronase at 4 hours post fertilization (hpf). Briefly, embryos were placed in 25 mL of FW with 50 μL of 50 mg/mL pronase (Fluka #81748) for 4-5 minutes; the water was decanted and replenished with fresh FW for a total of 10 minutes. Embryos were allowed to rest for at least 30 minutes prior to the initiation of nanoparticle exposure. After the rest period, dechorionated embryos were transferred to individual wells of a 96-well plate with 100 μL of prepared nanoparticle solution. Control

animals were exposed to FW only. Non-exposed animals (embryos raised in FW with the chorion intact) were also retained to monitor inherent embryo quality. Embryos were exposed to a FW control and six concentrations of nanoparticles (n=24, three replicates), with the highest concentration being 320 μg/mL (ppm) and the remainder from sequential two-fold dilutions down to 10 ppm. The static nanoparticle exposure continued under standard laboratory conditions in sealed plates until 120 hours post fertilization (hpf). Each individual embryo was scored for mortality and morphological malformations at 120 hpf. Only surviving embryos were accounted for when assessing for malformation. Fifteen morphological malformations were evaluated: yolk sac edema, bent body axis, eye, snout, jaw, otolith pericardial edema, brain, somite, caudal fin, pectoral fin, circulation, pigmentation, trunk length, and swim bladder. Representative images were captured of malformed embryos using an Infinity 3 CCD camera. The percent mortality and total malformations were calculated and graphed as a mean of three replicates with standard error bars.

Determination of Nanoparticle Uptake by ICP-MS—Embryos were exposed beginning at six hpf to PbS nanoparticle solutions of 10, 20, 40, 80, 160, and 320 μg/mL, and the embryos were sampled at 12 hpf to quantify their overall lead tissue concentrations. For each exposure group, three embryos were removed with plastic pipette tips and washed with 40 μL of Milli-Q water three times in a 35mm plastic petri dish. The pooled embryos were placed into individual 14mL round bottom plastic tubes and stored at −20°C until time to sample. Twelve hours prior to sampling, the embryos were digested using 98 μL nitric acid; 1 ppb of internal standard (Indium, Rhenium and Bismuth) was added; and, the samples were brought to a total volume of 5mL with Milli-Q water. Samples were vortexed for 10 seconds prior to being placed into the autosampler racks. The ICP-MS was calibrated using a lead standard in 0.5% HNO_3 at five concentrations (0.01, 0.1, 1, 5, 10 ppb) with 1 ppb internal standards. The calibration curve created by the standard solutions had an R^2 value of 0.992. The mass of lead contained in each embryo was calculated from the measured lead concentration of the aliquots and the dilution factor.

Statistics—All analyses were compiled using SigmaStat/Plot 11 (SPSS Inc, Chicago, IL). Dose response significance was determined using one-way ANOVA ($p<0.05$) and Dunnetts post hoc tests. All exposure groups consisted of 24 individually exposed embryos (N=24), three replicates unless otherwise noted with 80% confidence of significant difference.

Results

PbS Nanoparticles Synthesized through Ligand Exchange from a Common Core

Sodium 3-mercaptopropanesulfonate (MT), or sodium 2,3-dimercaptopropanesulfonate (DT) capped lead sulfide nanoparticles were synthesized (Figure 1a) and purified in an identical manner, using a biphasic exchange from oleic acid-capped lead sulfide nanoparticles (see Materials and Methods). Furthermore, each toxicological trial was performed using PbS-MT and PbS-DT nanoparticles prepared from the same parent batch of oleic-acid-capped nanoparticles. This was done to minimize the possibility that differences in biological response arose from different synthesis preparations. In addition, post-synthesis characterization of the nanoparticle cores was also conducted. Transmission electron microscopy (TEM) was used to image and calculate average nanoparticle sizes. Size analysis performed on TEM micrographs of representative samples of PbS-MT (Figures 1c) and PbS-DT (Figure 1d) revealed similar average particle diameters (3.0 and 3.5 nm, respectively). Corresponding near-infrared (NIR) absorption spectroscopy experiments (Figure 1b) showed close spectral overlap between the two materials, with exciton peaks observed at 1188 (PbS-MT) and 1202 nm (PbS-DT). Both TEM and NIR absorption

measurements were done on freshly-made particles and indicate initial properties. Precipitation of the nanoparticles over the course of the zebrafish exposures made post-exposure characterization infeasible.

PbS-MT, PbS-DT and Lead Nitrate Elicit Differential Biological Responses

Embryos were exposed to suspensions of lead sulfide nanoparticles capped with either the monothiol sodium 3-mercaptopropanesulfonate (PbS-MT) or the dithiol sodium 2,3-dimercaptopropanesulfonate (PbS-DT) over a two-fold concentration (10 - 320 μg/mL) range to determine if the nanoparticles elicited embryo mortality or induced developmental malformations. Exposure to PbS-MT induced mortality in 100% of the animals at 160 μg/mL (Figure 2a). At concentrations as low as 20 μg/mL, PbS-MT induced 20% mortality in the embryos, the remaining 80% survivors had an average of five malformations (Figure 2b). The multiple malformations observed upon PbS-MT exposure are visually represented in Figure 3b and include bent body axis, jaw, brain, and snout. At 40 and 80 μg/mL, the incidence of mortality was statistically significant ($p<0.001$) and increased to 75% and 92%, respectively. All surviving embryos exposed to PbS-MT displayed multiple malformations, with an average of 4.5 at 40 μg/mL (Figure 2b, 3b). Embryos exposed to PbS-DT nanoparticles, however, did not display statistically significant mortality at the same concentrations tested for PbS-MT (Figure 2a,b; 3c). PbS-DT exposed embryos had a consistent number of malformations (between 1.5 -2.3) at concentrations between 10 and 320 μg/mL, which is similar to that observed at higher concentrations (>80 μg/mL) for the ionic lead control sample, lead nitrate ($Pb(NO_3)_2$). The lead nitrate control was intended to model the extreme situation where the NPs entirely decomposed into water soluble lead salts, which is admittedly unlikely given the insolubility of PbS (K_{sp} of 2.5×10^{-27}). Lead nitrate is soluble in pure water, but the presence of carbonate and other anions in the FW used for the experiments leads to some precipitation. Further, the addition of $Pb(NO_3)_2$ also results in acidification of the FW to as low as 5.2 at the highest concentrations. It is noted that PbS-MT and Pb-DT are soluble in FW at the concentrations used in this study, and their addition does not affect the pH. The various equilibria involving lead ion in FW means that the listed concentrations for $Pb(NO_3)_2$ do not necessarily represent the concentration of freely soluble lead. Nevertheless, $Pb(NO_3)_2$ remains a good control because the same equilibria affecting its bioavailability also operate on any ionic lead leached from the nanoparticles. The onset of mortality in $Pb(NO_3)_2$ exposures occurred at a greater concentration than that observed for PbS-MT exposures. Embryos exposed to 10–40 μg/mL of lead nitrate had 0.25 or fewer malformations, but the average number of malformations rose to 2.3 at 160 μg/mL. Lead nitrate induced a statistically significant increase in bent body axis in the embryo (Figure 3d) at 160 μg/mL. Near 320 μg/mL, 100% mortality was observed for both $Pb(NO_3)_2$ and PbS-MT. At this concentration, no significant mortality was observed for PbS-DT exposures.

Monothiol and Dithiol Ligands Did Not Induce Biological Responses

To determine if the ligands themselves were responsible for the adverse biological response, embryonic zebrafish were exposed to MT and DT ligands independent of the nanoparticles. Both ligands were tested at the same concentrations used for the nanoparticle exposures. These concentrations were greater than the ligand concentrations in the corresponding nanoparticle solutions, since the ligands make up only a fraction of the nanoparticle-ligand complex. As seen in Figures 2c, and d, there was no statistically significant increase in malformation or mortality observed in embryos exposed to the ligands.

PbS-MT Nanoparticles Decomposed More Readily Than PbS-DT

PbS-MT and PbS-DT nanoparticles are known to precipitate from aqueous solution upon exposure to air, however, the effects of salinity from exposure to FW were hitherto

unexplored. To test the relative stabilities of PbS-MT and PbS-DT nanoparticles in FW, dynamic light scattering (DLS) measurements were performed. Although zebrafish exposures were made using unfiltered nanoparticle solutions, DLS measurements required pre-filtering to remove dust that could affect the scattering experiments. Hydrodynamic radii were measured at times 0, 24, 48, and 120hr. Both samples showed evidence of agglomeration with hydrodynamic radii greater than the average nanoparticle diameter. However, PbS-MT exhibited greater particle size and destabilized more quickly than the PbS-DT samples. PbS-DT samples maintained a consistent particle size of ~80 nm at 0, 24, and 48hr, but had completely precipitated by 120hr. Conversely, PbS-MT samples had average hydrodynamic radii of 140 nm at 0 hr and 340 nm at 24hr, and had completely precipitated by 48hr.

It was hypothesized that degradation of the nanoparticle cores could follow precipitation and give rise to ionic lead decomposition products. To quantify the concentration of ionic lead after five-day exposure to air (aged), nanoparticle solutions were monitored using an Inductively Coupled Plasma – Optical Emission Spectrometer (ICP-OES). Aged solutions were first centrifuged to remove insoluble species (i.e. precipitated nanoparticles), and the resulting supernatant digested with nitric acid. The lead content in the supernatants of the aged nanoparticle solutions was 87 +/− 0.4 ppm (4% recovery rate) for PbS-MT, and 1.075 +/− 0.002 ppm (0.02% recovery rate) for PbS-DT, a statistically significant difference. It is important to note that the 87 ppm lead content measured for the aged PbS-MT sample is not due to the original nanoparticles; fresh solutions of PbS-MT nanoparticles at this concentration are clearly colored due to absorption from the nanoparticle core, whereas the supernatant was colorless. Precaution was taken to ensure that differences in lead concentration seen in the supernatants of the aged solutions was not simply due to different starting concentrations of nanoparticles in the fresh solutions. As a control, aliquots of the fresh nanoparticle solutions were digested with nitric acid, and the total lead content measured in an analogous manner using ICP-OES. Analysis of the fresh nanoparticle solutions revealed a similar amount of lead present for the two materials (Figure 4). PbS-MT had 1927 +/− 7 ppm of lead while PbS-DT had 2270 +/− 10 ppm (Figure 4a), corresponding to approximately 90% and 110% recovered lead for PbS-MT and PbS-DT, respectively (Figure 4b). This study demonstrates that the nanoparticles were decomposing over time, releasing ionic lead into solution.

Lead Quantified in PbS-MT, PbS-DT and Lead Nitrate Exposed Embryos

Inductively Coupled Plasmas – Mass Spectrometry (ICP-MS) was used to quantify the amount of lead in or tightly associated to the embryo. These measurements were done to determine if the differential biological response to the PbS could be explained by differences in particle uptake. Embryos were exposed to concentrations (0 – 320 μg/mL) of either PbS-MT, PbS-DT, or $Pb(NO_3)_2$ and samples were collected at 12 hpf. At this developmental time point, there was no strict dose-dependent increase in lead uptake at low concentration; however, there was a significant increase in lead concentration following 160 μg/mL lead exposure for PbS-MT. A dose-dependent increase in the tissue concentration of lead was observed in the PbS-DT and $Pb(NO_3)_2$ exposed embryos (Figure 5). PbS-DT exposed embryos had the highest lead level for all concentrations up until 160 μg/mL, where PbS-MT embryos had significantly more lead tissue burden.

Discussion

In this *in vivo* study, we find that the biological response following exposure to lead sulfide nanoparticles (PbS-NPs) is influenced greatly by surface functionalization. Two major effects can be gleaned from the exposure trials. First, DT-functionalized PbS nanoparticles (PbS-DT) elicit fewer responses than MT-functionalized PbS nanoparticles (PbS-MT).

Exposure to PbS-MT induces 100% mortality at 160 μg/mL in zebrafish embryos at 120 hpf and also a variety of sublethal malformations. Conversely, embryos exposed to PbS-DT elicit little to no mortality and fewer sublethal adverse responses. Second, PbS-MT exposure causes significantly more, and PbS-DT significantly less, mortality than the ionic lead source, lead nitrate ($Pb(NO_3)_2$). PbS-MT and $Pb(NO_3)_2$ exposed embryos were morphologically similar at concentrations near the onset of mortality. The simplest explanation for these results is a correlation between toxicity and nanoparticle stability. Destabilization of the nanoparticles occurs over the course of the exposure. The two ligands offer differential resistance to this destabilization, leading to differential biological responses in the embryos.

Nanoparticle stability can greatly influence exposure of the core surface. Thiolate ligands at the metal chalcogenide nanoparticle-ligand interface are susceptible to oxidative decomposition (Aldana et al. 2001, Moody et al. 2008). This instability can lead to ligand desorption, resulting in particle agglomeration, greater exposure of the nanoparticle core, and decomposition of the core with the possible generation of soluble ionic lead species.

To our knowledge, no prior toxicity studies have been conducted on PbS-NPs; however, lessons can be learned from studies on other material sets. In general, nanoparticles have been observed to cause cytotoxicity (Lewinski et al. 2008), oxidative stress (Long et al. 2006), and immune responses (Dobrovolskaia and McNeil 2007), either through biochemical interactions with the nanoparticles themselves or from their toxic decomposition products. The ligand shell can influence toxicity by affecting nanoparticle uptake and distribution in biological systems (Goldsmith and Leary 2009) or as an integral part of the entire nanoparticle-ligand assembly. The accessibility of the nanoparticle core has also been implicated as a potentially important factor. Nanoparticles that have a denser coverage of surface ligands, or are encapsulated by an inert material (Zhang et al. 2006), are generally less toxic than those particles that offer greater access to the core.

Prior comparisons between PbS-MT and PbS-DT nanoparticles have shown that both materials are susceptible to oxidative decomposition in aqueous solution (Moody et al. 2008). Specifically, the thiol head groups of both MT and DT ligands oxidize to form disulfides, which bind poorly to the nanoparticle surface. The MT ligands oxidize relatively quickly, resulting in rapid ligand desorption and nanoparticle precipitation. Oxidation of the DT ligands proceeds more slowly, and in a manner, which leaves the ligands partially attached to the nanoparticle surface. Although these studies were not conducted in fish water, they suggest that differential decomposition could play a role in the observed biological effects.

In this study, differential stability resulting from different surface functionalization is implicated as the major contributor to the differential biological response to the nanoparticles. DLS measurements performed on nanoparticles in fish water showed that although solution salinity affects agglomeration, PbS-DT nanoparticles are more stable than PbS-MT nanoparticles, just as in prior studies using nanoparticle solutions in deionized water. Core size was not a significant variable in the differential response. Direct comparisons of PbS-MT and PbS-DT nanoparticles were conducted using nanoparticles prepared from the same OLA-capped precursor, and exhibited similar core-related properties. Effects from the ligands themselves were also ruled out as significant factors, as they induce no to low incidence of mortality and morbidity. It is certainly possible that the differential response of the nanoparticles is due to differences in the biological interactions of the entire intact nanoparticle structure. We look to oxidative stability as the likely differentiator, however, because it is the most notable difference in the physicochemical

properties of the nanoparticles. The differential oxidative stability is due to the ligand head group (monothiol vs. dithiol).

The mechanism for how the different decomposition rates of PbS-MT and PbS-DT result in differential nanoparticle-biological interactions remains unclear. Two likely causes for the toxicity are interactions with either 1) presumably ionic lead decomposition products or 2) the exposed nanoparticle cores. The primary reason the interaction cannot be distinguished is the challenge of quantifying dose. Two studies shed light on the dose of either nanoparticles or its decomposition products received by the embryos. The first is the ICP-OES measurements performed on aged nanoparticle solutions. Soluble lead products are observed during the oxidative decomposition and precipitation of the nanoparticles, with a much greater concentration of ionic lead observed for PbS-MT relative to PbS-DT. Analysis of the fresh PbS-MT and PbS-DT solutions began with similar concentrations of nanoparticles. However, analysis of the aged solutions show that the two ligands are not equal in their protection of the nanoparticle surface; as they decompose and precipitate, MT-capped nanoparticles leach ~ 80 times more ionic lead into solution than DT-capped nanoparticles. As the PbS-NP solutions age, ligands are oxidized and desorb from the nanoparticle surface, resulting in nanoparticle precipitation. During this process, lead can leach from exposed sites on the nanoparticle cores. The concentration of soluble lead decomposition products observed in the aging studies was below the onset of toxicity at 160 μg/mL for $Pb(NO_3)_2$, even given the much higher concentration (3000 μg/mL) of nanoparticles used for the ICP-OES studies than for the toxicity studies. What is important, however, is not simply the concentration of soluble lead in the fish water but the actual dose received by the embryos. This dose is dependent on the distribution of nanoparticles, which suggests that the PbS-NPs are associating with the embryos in the exposure media and resulting in localized soluble lead decomposition products.

Tissue uptake studies were performed in an attempt to better define the dose. In these studies, exposed embryos were washed and then analyzed for lead content using ICP-MS. One limitation of this technique is that no distinction can be made between lead tightly bound to, or within the embryo. Visual inspections of the embryos after exposure revealed signs of adsorbed nanoparticles. It is hypothesized that at higher concentrations, nanoparticle solutions are more susceptible to agglomeration, and that these agglomerates may adhere preferentially to the embryos. This effect would substantially increase the local concentration of lead around the embryos, leading to increased uptake relative to a uniform solution distribution. Note that the uptake studies were performed at early exposure times. At these early times, only the PbS-MT induced substantial mortality at 320 μg/mL. Near the onset of this mortality (160 μg/mL), the PbS-MT nanoparticles exhibited a sharp increase in uptake to levels higher than those observed for either the PbS-DT or $Pb(NO_3)_2$ exposures.

The uptake and decomposition studies do not definitively distinguish between direct nanoparticle toxicity and nanoparticle decomposition product toxicity. The differential toxicity of the PbS-MT vs. PbS-DT nanoparticles can be explained by greater exposure of the nanoparticle core in the former during decomposition. This mechanism also provides a simple explanation for the greater toxicity of the PbS-MT nanoparticles relative to $Pb(NO_3)_2$. Alternatively, nanoparticle decomposition products could be responsible for the increased toxicity of PbS-MT relative to PbS-DT consistent with the greater amount of lead observed to leach from aged solutions of the PbS-MT. The enhanced toxicity of PbS-MT relative to $Pb(NO_3)_2$ is explained by the agglomeration of nanoparticles on or in the embryos, which acts to increase the local lead concentration. Such a local increase is consistent with the substantial lead uptake observed near the onset of toxicity (160 μg/mL) in the 12 hpf uptake studies.

Further studies will be needed to differentiate between the biological interactions with either the nanoparticle cores and/or soluble decomposition products. Regardless, these studies illustrate the substantial changes in nanoparticle toxicity that can be induced by a relative minor change in ligand composition. With the knowledge that manipulating physicochemical properties of nanoparticles results in differential biological responses, a systematic methodical use of the rapidly developing embryonic zebrafish model will aid in elucidating the key design principles to develop minimal to non-toxic nanoparticles.

Additionally, these studies using the PbS-NPs highlight the important role nanoparticle decomposition plays in toxicity. The possibility of ionic lead leaching from the nanoparticles also suggests that more studies should be conducted to understand the poorly-known mechanisms of lead toxicity. Physicochemical characterization of NPs in their synthesis media is important, but as demonstrated in these studies, it is critical to conduct characterization of the NPs in exposure media in parallel to toxicity assessments to gain a better understanding of aggregation state and other physicochemical properties. As the field of nanotechnology expands and matures, greater understanding of the nanomaterial-biological interface will be imperative.

Conclusions

The data presented demonstrates the usefulness of the embryonic zebrafish model as a platform to rapidly assess the nanomaterial-biological interaction of nanoparticles. With this set of nanoparticles, different biological responses between PbS-MT and PbS-DT nanoparticles was attributed to differences in their rates of decomposition. This study illustrates the importance of using well-characterized nanoparticles both from the start, as well as over time. It also opens discussion on the hitherto unexplored biological interactions of lead sulfide nanoparticles. Use of the embryonic zebrafish to conduct nanomaterial-biological interaction assessments will increase the speed at which key physicochemical properties will be identified and used to implement a design rule to produce safer nanomaterials.

Acknowledgments

We would like to thank Sinnhuber Aquatic Research Laboratory for the embryos and Cari Buchner for her technical assistance. These studies were partially supported by National Institute of Environmental Health Sciences (NIEHS) P3000210, the Air Force Research Laboratory (AFRL) under agreement number FA8650-05-1-5041, Environmental Protection Agency (EPA) RD-833320, and the National Science Foundation (NSF) IGERT Fellowship program under Grant No. DGE-0549503. The views and conclusions contained herein are those of the authors and should not be interpreted as necessarily representing the official policies or endorsements, either expressed or implied, of NIEHS, AFRL, EPA, NSF or the U.S. Government. Further support was provided by the W.M Keck Foundation.

References

Agency for Toxic Substances and Disease Registry (ATSDR). Toxicological profile for lead. Atlanta, GA: U.S. Department of Health and Human Services, Public Health Service; 2007.

Aldana J, Wang Y, Peng X. Photochemical Instability of CdSe Nanocrystals Coated by Hydrophillic Thiols. Journal of the American Chemical Society. 2001; 123(36):8844–8850. [PubMed: 11535092]

Barbazuk WB, Korf I, et al. The syntenic relationship of the zebrafish and human genomes. Genome Res. 2000; 10(9):1351–8. [PubMed: 10984453]

Bharali DJ, Khalil M, et al. Nanoparticles and cancer therapy: A concise review with emphasis on dendrimers. International Journal of Nanomedicine. 2009; 4(1):1–7. [PubMed: 19421366]

De Gennardo LD. The effects of lead nitrate on the central nervous system of the chick embryo I. Observations of light and electron microscopy. Growth. 1978; 42(2):141–55. [PubMed: 680579]

den Hertog J. Chemical Genetics: Drug screens in Zebrafish. Biosci Rep. 2005; 25(5–6):289–97. [PubMed: 16307377]

Dobrovolskaia MA, McNeil SE. Immunological properties of engineered nanomaterials. Nature Nanotechnology. 2007; 2(8):469–478.

Dodd A, Curtis PM, et al. Zebrafish: bridging the gap between development and disease. Hum Mol Genet. 2000; 9(16):2443–9. [PubMed: 11005800]

Furgeson D, Barllan O, et al. Toxicity Assessments of Multisized Gold and Silver Nanoparticles in Zebrafish Embryos. Small. 2009; X:1–14.

Goldsmith M-M, Leary J. Nanobiosystems. WIREs Nanomed Nanobiotechnology. 2009; 1:553–567.

Guo L, Bussche AV, et al. Adsorption of essential micronutrients by carbon nanotubes and the implications for nanotoxicity testing. Small. 2008; 4(6):721–727. [PubMed: 18504717]

Haendel MA, Tilton F, et al. Developmental toxicity of the dithiocarbamate pesticide sodium metam in zebrafish. Toxicological Science. 2004; 81(2):390–400.

Hall JB, Dobrovolskaia MA, et al. Characterization of nanoparticles for therapeutics. Nanomedicine (Lond). 2007; 2(6):789–803. [PubMed: 18095846]

Hill AJ, Teraoka H, et al. Zebrafish as a model vertebrate for investigating chemical toxicity. Toxicological Sciences. 2005; 86(1):6–19. [PubMed: 15703261]

Hinds S, Myrskog S, Levina L, Koleilat G, Yang J, Kelley SO, Sargent EH. NIR-Emitting Colloidal Quantum Dots Having 26% Luminescence Quantum Yield in Buffer Solution. Journal of the American Chemical Society. 2007; 129(23):7218–7219. [PubMed: 17503821]

Hoshino A, Fujioka K, et al. Physicochemical properties and cellular toxicity of nanocrystal quantum dots depend on their surface modification. Nano Letters. 2004; 4(11):2163–2169.

Hyun B, Chen H, Rey DA, Wise FW, Batt CA. Near-Infrared Fluorescence Imaging with Water-Soluble Lead Salt Quantum Dots. Journal of Physical Chemistry B. 2007; 111(20):5726–5730.

Kimmel CB, Ballard WW, et al. Stages of embryonic development of the zebrafish. Dev Dyn. 1995; 203(3):253–310. [PubMed: 8589427]

Kirchner C, Liedl T, et al. Cytotoxicity of colloidal CdSe and CdSe/ZnS nanoparticles. Nano Letters. 2005; 5(2):331–338. [PubMed: 15794621]

Koleilat GI, Levina L, et al. Efficient, stable infrared photovoltaics based on solution-cast colloidal quantum dots. ACS Nano. 2008; 2(5):833–40. [PubMed: 19206479]

Konstantatos G, Huang C, Levina L, Lu Z, Sargent EH. Efficient Infrared Electroluminescent Devices Using Solution-Processed Colloidal Quantum Dots. Advanced Functional Materials. 2005; 15:1865–1869.

Konstantatos G, Howard I, et al. Ultrasensitive solution-cast quantum dot photodetectors. Nature. 2006; 442(7099):180–3. [PubMed: 16838017]

Kotov NA, Winter JO, et al. Nanomaterials for Neural Interfaces. Advanced Materials. 2009; 21(40): 3970–4004.

Lewinski N, Colvin V, et al. Cytotoxicity of nanoparticles. Small. 2008; 4(1):26–49. [PubMed: 18165959]

Long TC, Saleh N, et al. Titanium dioxide (P25) produces reactive oxygen species in immortalized brain microglia (BV2): Implications for nanoparticle neurotoxicity. Environmental Science & Technology. 2006; 40(14):4346–4352. [PubMed: 16903269]

Lim YT, Kim S, Nakayama A, Stott NE, Bawendi MG, Frangioni JV. Selection of Quantum Dot Wavelengths for Biomedical Assays and Imaging. Molecular Imaging. 2003; 2(1):50–64. [PubMed: 12926237]

Liu J, Aruguete DM, Murayama M, Hochella MF Jr. Influence of Size and Aggregation on the Reactivity of an Environmentally and Industrially Relevant Nanomaterial (PbS). Environmental Science & Technology. 2009; 43(21):8178–8183. [PubMed: 19924941]

McDonald SA, Konstantatos G, et al. Solution-processed PbS quantum dot infrared photodetectors and photovoltaics. Nat Mater. 2005; 4(2):138–42. [PubMed: 15640806]

Meng H, Chen Z, et al. Ultrahigh reactivity provokes nanotoxicity: Explanation of oral toxicity of nano-copper particles. Toxicology Letters. 2007; 175(1–3):102–110. [PubMed: 18024012]

Minchin RF, Martin DJ. Nanoparticles for molecular imaging--an overview. Endocrinology. 2010; 151(2):474–81. [PubMed: 20016027]

Moody IS, Stonas AR, et al. PbS Nanocrystals Functionalized with a Short-Chain, Ionic, Dithiol Ligand. Journal of Physical Chemistry C. 2008; 112(49):19383–19389.

Newman MD, Stotland M, et al. The safety of nanosized particles in titanium dioxide-and zinc oxide-based sunscreens. Journal of the American Academy of Dermatology. 2009; 61(4):685–692. [PubMed: 19646780]

Parng C. In vivo zebrafish assays for toxicity testing. Curr Opin Drug Discov Devel. 2005; 8(1):100–6.

Rubinstein AL. Zebrafish: from disease modeling to drug discovery. Curr Opin Drug Discov Devel. 2003; 6(2):218–23.

Samia ACS, Chen XB, et al. Semiconductor quantum dots for photodynamic therapy. Journal of the American Chemical Society. 2003; 125(51):15736–15737. [PubMed: 14677951]

Sharma V, Sharma A, Kansal L. The effect of oral administration of Allium sativum extracts on lead nitrate induced toxicity in male mice. Food Chemical Toxicity. 2010; 48(3):928–36.

Teraoka H, Dong W, et al. Zebrafish as a novel experimental model for developmental toxicology. Congenit Anom (Kyoto). 2003; 43(2):123–32. [PubMed: 12893971]

Ton C, Lin Y, et al. Zebrafish as a model for developmental neurotoxicity testing. Birth Defects Research A Clin Mol Teratol. 2006; 76(7):553–67.

Usenko CY, Harper SL, et al. In vivo evaluation of carbon fullerene toxicity using embryonic zebrafish. Carbon N Y. 2007; 45(9):1891–1898. [PubMed: 18670586]

Wise JP Sr, Goodale BC, et al. Silver nanospheres are cytotoxic and genotoxic to fish cells. Aquatic Toxicology. 2009; 97(1):34–41. [PubMed: 20060603]

White D, Cory-Slechta A, Gilbert E, Tiffany-Castiglioni E, Zawai H, Virgolini M, Rossi-George A, Lasley M, et al. New and evolving concepts in the neurotoxicology of lead. Toxicology and Applied Pharmacology. 2007; 225(1):1–27. [PubMed: 17904601]

Yang LX, Ho NY, Alshut R, Legradi J, Weiss C, Reischl M, Mikut R, Liebel U, Muller F, Strahle U. Zebrafish embryos as models for embryotoxic and teratological effects of chemicals. Reproductive Toxicology. 2009; 28(2):245–253. [PubMed: 19406227]

Zelikoff JT, Li JH, Hartwig A, Wang XW, Costa M, Rossman TG. Genetic toxicology of lead compounds. Carcinogenesis. 1988; 9(10):1727–32. [PubMed: 3168150]

Zhang TT, Stilwell JL, et al. Cellular effect of high doses of silica-coated quantum dot profiled with high throughput gene expression analysis and high content cellomics measurements. Nano Letters. 2006; 6(4):800–808. [PubMed: 16608287]

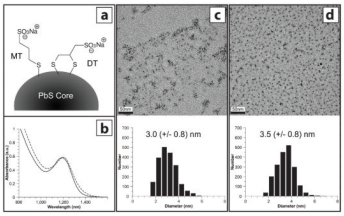

Figure 1. Physical Properties of PbS-MT and PbS-DT Nanoparticles

(a) Schematic of two ligands used in the study – sodium 3-mercaptopropane sulfonate (MT) and sodium 2,3-dimercaptopropane sulfonate (DT). **(b)** Near-infrared absorption spectra of solutions of PbS-MT(*solid*) and PbS-DT (*dashed*) nanoparticles. Peak position is indicative of average particle size. Plots were scaled to better illustrate spectral overlap. (**c** and **d**) TEM images of PbS-MT and PbS-DT, respectively, with corresponding particle size histograms. Scale bars represent 50 nm. Values in histograms show average nanoparticle diameter, with standard deviation in parentheses.

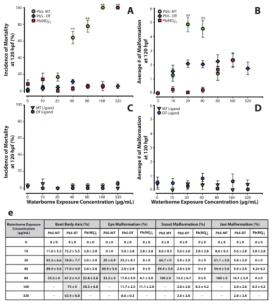

Figure 2. Mortality and Malformation Curves for Embryos Exposed to PbS-MT, PbS-DT, $Pb(NO_3)_2$, and MT and DT Ligands

Embryos were exposed to PbS-MT, PbS-DT or $Pb(NO_3)_2$ at 6 hpf and were evaluated for malformations and mortality at 120 hpf. Mortality (a) was statistically significant for PbS-MT (40 - 320 μg/mL) and $Pb(NO_3)_2$ (only at 320 μg/mL). All surviving embryos exposed to PbS-MT had malformations (average of 5 at 20 μg/mL) **(b)**. $Pb(NO_3)_2$ exposed embryos had little to no malformations (<0.25) up until 40 μg/mL, where a steady increase of malformations was observed at 80 and 160 μg/mL. PbS-DT exposed embryos caused a consistent number of malformations (~2) at all concentrations. A summary of the statistically significant malformations observed in PbS-MT, PbS-DT and $Pb(NO_3)_2$ exposed embryos is visualized in a table **(e),** where shaded boxes indicate statistical significance (Fishers Exact, $p<0.05$). MT and DT ligands did not induce mortality **(c)** or malformations **(d)** in exposed embryos. Data presented with ** designate statistically significant values (Fishers Exact, **$p<0.001$). Three replicates, n=24.

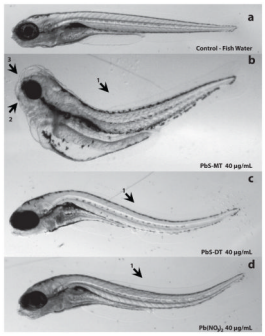

Figure 3. Representative Images of Exposed Zebrafish Embryos

Embryonic zebrafish exposed to PbS-MT nanoparticles (**b**) and $Pb(NO_3)_2$ (**d**) induced a statistically significant increase in bent body axis (1), jaw (2) and snout (3) malformation compared to control (**a**). PbS-DT (**c**) elicited a statistically significant increase in bent body axis, and jaw malformation, but not snout abnormalities. All images were taken at 120 hpf, and except for the control embryo, represent exposures at a concentration of 40 μg/mL.

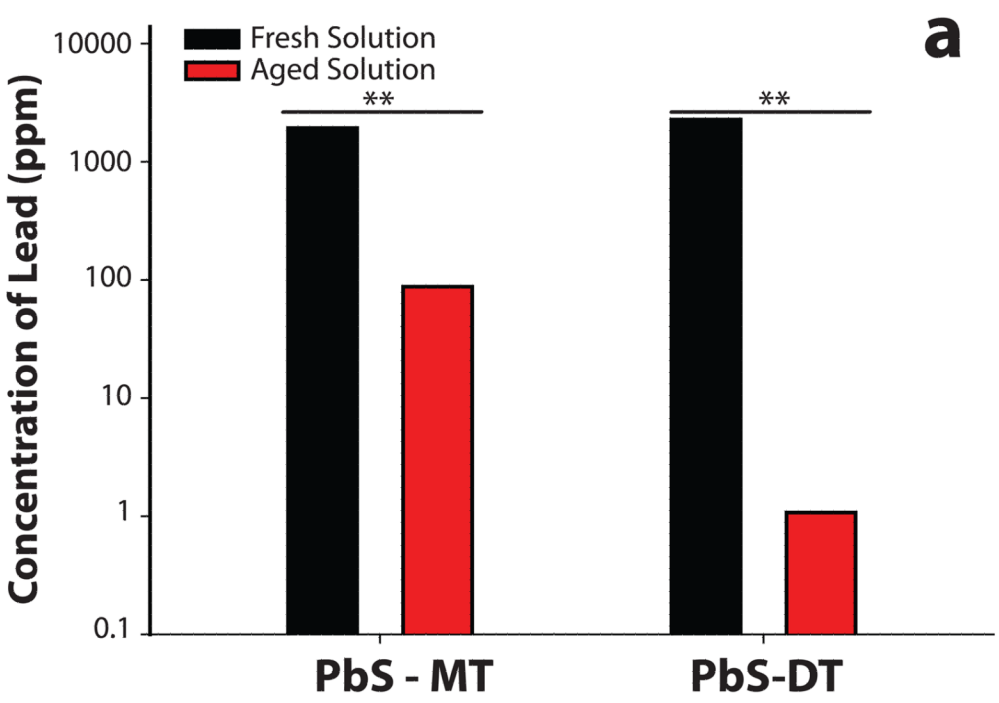

b

	PbS-MT	PbS-DT
Theoretical Concentration of Pb (ppm)	2189	2129
Measured Concentration of Fresh Solution (ppm)	1927 ± 7	2270 ± 10
Pb Recovered (%)	90%	110%
Measured Concentration of Aged Solution (ppm)	87 ± 0.4	1.075 ± 0.002
Pb Recovered (%)	4%	0.02%

Figure 4. Concentration of Lead (Pb) in Fresh and Aged PbS-MT and PbS-DT Solutions

Nanoparticle solutions that were initially opened (fresh) and left to oxidize for 5 days (aged) were digested with nitric acid, and Pb concentration was measured 18 hours later **(a)** with ICP -Optical Emission Spectrometer (OES). Expected Pb percent recovery concentrations were calculated for both nanoparticles for fresh and aged solutions **(b).** Data presented with ** designate statistically significant values (Student t-Test, **p<0.001).

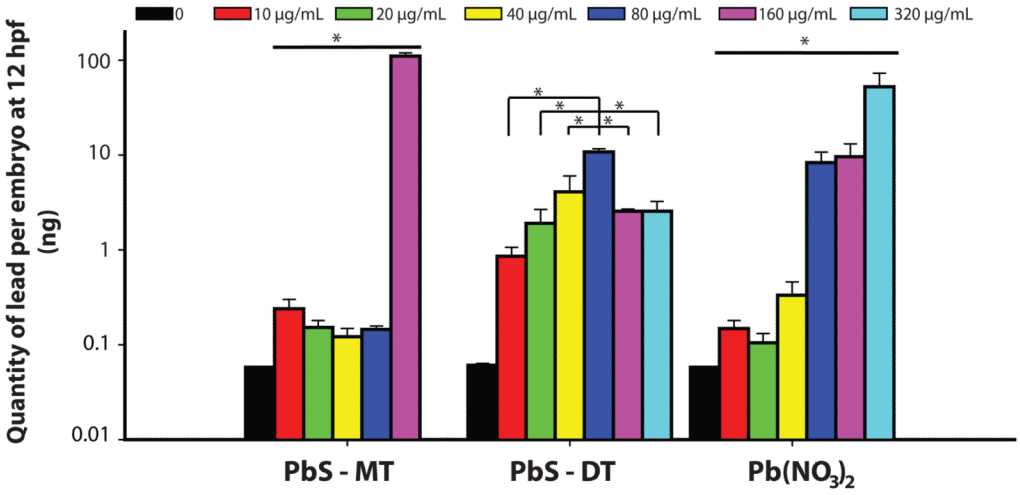

Figure 5. Tissue Concentration of Lead in Embryos Exposed to PbS-MT, PbS-DT and $Pb(NO_3)_2$

Embryos were exposed to 10 - 320 µg/mL solutions of PbS-MT, DT, and $Pb(NO_3)_2$ at 6 hpf and sampled at 12 hpf. Embryos exposed to PbS-MT at 320 µg/mL did not survive to the time of sampling. Both $Pb(NO_3)_2$ and PbS-DT tissue concentration followed a dose dependent manner, except PbS-DT only followed this trend until 80 µg/mL. Data presented with * designate statistically significant values (Kruskal-Wallis ANOVA - Tukey Test, $p<0.05$).